Valentino, G. et al. (2023). *Xjenza Online*, 11 Special Issue: 49–58.

Xjenza Online: Science Journal of the Malta Chamber of Scientists
www.xjenza.org
DOI: 10.7423/XJENZA.2023.1.06

Review Article

Interferometric phase denoising and unwrapping: a literature review

G. Valentino[*1], **J. A. Briffa**[1], **R. Farrugia**[1], **A. Fejjari**[1]
[1] *Department of Communications and Computer Engineering, University of Malta, Msida, Malta*

Abstract. Interferometric SAR (InSAR) phase denoising and phase unwrapping are two key steps of the InSAR pipeline, leading to estimated deformation maps. The objective of this paper is to provide an overview of the recent literature in the field of InSAR phase denoising and unwrapping, and identify the most promising techniques, as well as benchmarks for performance comparison. Summaries of the performance metrics of the various methods are also provided. An example use case of InSAR techniques, including phase denoising and unwrapping, to estimate deformation following a volcanic eruption is provided.

Keywords: InSAR, phase denoising, phase unwrapping

1 Introduction

Freely-available satellite data provides a wealth of regularly updated data which can be used to monitor effects of coastal erosion and provide an early warning system against hazards. As opposed to optical and thermal satellite imagery, Synthetic Aperture Radar (SAR) images are produced by active remote sensing, in which microwaves are beamed from the satellite towards Earth, and the reflected waves are detected by sensors onboard the satellite. Ground displacements of a few millimeters from one time-series image to another can be detected. The advantages of SAR remote sensing is that images can be acquired in any type of weather conditions, day or night.

The Copernicus programme's Sentinel-1 satellite constellation (European Space Agency, 2012) provides C-band SAR capability, with a repeat frequency of 6 days and a revisit frequency of around 2 days over Europe. The data is acquired in four modes: Extra Wide (EW) Swath mode (spatial resolution: 25 m x 100 m), Interferometric Wide (IW) Swath mode (spatial resolution: 5 m x 20 m), Strip Map (SM) mode (spatial resolution: 5 m x 5 m) and Wave (WV) mode (spatial resolution: 5 m x 20 m, mainly used over open ocean). The Stripmap mode is only available for emergency situations and certain select geographical locations (and is not available online for Malta through the Copernicus Open Access Hub (European Space Agency, 2022)). The IW mode is the one typically used for interferometric analysis and land subsidence detection.

An Interferometric SAR (InSAR) image, also known as an interferogram, is created from two temporally separated single look complex (SLC) SAR images via the pixel-wise product of one SLC image with the complex conjugate of the other SLC image. Thus each pixel in an interferogram indicates the phase difference between two co-registered SLC images. The phase difference encodes useful information including deformation of the earth's surface. A differential interferogram is created when an external DEM is used to subtract the topographic information from the interferogram.

At this point, it is vital to denoise the resulting interferogram, as in particular the phase noise will significantly affect all subsequent stages from phase unwrapping to motion signal modelling. The phase noise can be modeled as additive noise. The classical and most widespread denoising approach is to use a multilook filter (Jong-Sen Lee et al., 1994a), which applies a simple moving average on neighbour pixels in a rectangular window, i.e. boxcar filtering. The disadvantages of the multilook filter are the resolution loss and phase fringe distortion when dealing with the high-topography and high-heterogeneity areas. The multilook filter assumes that the interferometric phase is locally stationary and the scene reflectivity is homogeneous in a local window, where the selected samples are independently and identically distributed (i.i.d.). In this case, the multilook filter expects to perform a maximum likelihood (ML) estimation (Seymour et al., 1994), which is also the foundation of most phase filtering methods.

**Correspondence to*: G. Valentino (gianluca.valentino@um.edu.mt)

However, this assumption is not always true due to the topography variation and reflectivity heterogeneity, especially when faced with the scenes of region edge, structure and texture. In this case, the interferometric phase tends to exhibit the characteristics of nonstationarity and nonhomogeneity, conflicting with the i.i.d. assumption.

The accuracy of the phase measurement in the interferogram is limited by the magnitude of the interferometric coherence, which describes the degree of correlation between the two radar images. There are a number of factors which contribute to a reduction of coherence, including receiver noise, temporal and geometric decorrelation. Therefore, the estimated coherence map of an interferogram is a crucial indicator showing the reliability of the interferometric phase.

The produced interferograms consist of a wrapped phase limited to the interval (-π, π], resulting in phase discontinuities. Phase unwrapping is then computed to obtain the true phase, which is generally considered to be the most complicated stage of InSAR processing. This is however a necessary step in order to obtain height information. Single baseline phase unwrapping is an ill-posed inverse problem, as there are infinite solutions. The SNAPHU plugin for SNAP is a widely used tool to perform 2D phase unwrapping (C. W. Chen et al., 2002). It treats phase unwrapping as a maximum a posteriori probability estimation problem, and tries to compute the most likely unwrapped solution given the data available. The optimization problem is solved approximately using network-flow techniques.

In this paper, we review a number of state-of-the-art methods for InSAR phase denoising and unwrapping, and provide a comparison between the methods in each case using appropriate metrics. In addition, as an example, we show how these techniques can be applied to estimate the deformation that occurred at Mount Etna following an eruption in December 2018.

2 Denoising of SAR interferometric phase

2.1 Methods

There are several works in the literature which focus on, as well as a number of EO processing pipelines which support denoising (or restoration) of interferometric phase. The boxcar filter (Jong-Sen Lee et al., 1994b) is a well-known method, which simply performs a moving average to estimate the variation of the local pixel pattern. However, it results in a loss of spatial resolution, and it is not suitable for areas with large slopes. The Lee filter (Jong-Sen Lee et al., 1998) is another well-known classical method. It takes advantage of the local fringe morphology and reduces the noise via local statistics and an adaptive window. On the other hand, the Goldstein filter is a frequency domain method (Goldstein et al., 1998). As part of its SAR interferometry processing chain, SNAP has inbuilt functionality for denoising after generating an interferogram. This involves performing multilook processing followed by applying a filter (such as the Goldstein filter).

Following the realization that clean signal phase values are also correlated in the temporal domain, in recent years, many methods have started taking the interferogram stack into consideration. Theoretically, it is easier to extract displacement information over a longer period of time. DespecKS (Ferretti et al., 2011) introduced a space adaptive processing together with their SqueeSAR procedure that could filter interferometric phase properly by using amplitude SAR images.

Another modern concept is that of nonlocal filtering, where the idea is to exploit further information from the data itself. In general, images contain repetitive structures such as corners and lines. Those redundant patterns in an image could be analyzed and explored to improve filtering performance. More and more studies are deploying nonlocal techniques for interferometric phase denoising (R. Chen et al., 2013; Deledalle et al., 2011; Zhu et al., 2014). The first nonlocal method applied to interferometric phase filtering was proposed by Deledalle et al., 2009. Both image intensities and interferometric phase information are used to build a nonlocal means model with a probability criterion for estimating pixels. NL-InSAR (Deledalle et al., 2011) is the first InSAR application to use a non-local approach for the joint estimation of the reflectivity, interferometric phase and coherence map from a pair of coregistered SLC SAR images. In (R. Chen et al., 2013) and Lin et al., 2015, researchers achieve better results on textural fine details preservation by combining non-local filtering with other conventional natural image processing algorithms, such as pyramidal representation and singular value decomposition. A unified framework (NL-SAR) is proposed in (Deledalle et al., 2015) as an extension of NL-InSAR, where an adaptive procedure is carried out to handle very high resolution images. It is able to obtain the best nonlocal estimation with good quality on radar structures and discontinuities reconstruction.

Another popular algorithm, nonlocal block-matching 3D (BM3D) which is widely used for additive white Gaussian noise removal for natural images, also inspired researchers to propose InSAR-BM3D (Sica et al., 2018) which delivered state-of-the-art results for InSAR phase filtering. The method is not able to concurrently estimate phase coherence. Instead, InSAR-BM3D requires a coherence map as input and as a result, the performance is likely affected by the accuracy of the coherence estimator.

Recently, machine learning methods have also demonstrated excellent performance in the task of image restoration and denoising. A number of these techniques have also been applied to the problem of interferometric phase denoising. In (Kang et al., 2021), the authors propose a complex convolutional sparse coding algorithm, which avoids staircase effects and preserves the details of phase variations. A Fully Convolutional Network is used in (Li et al., 2019) to segment layover areas from the normal pixels, and a denoising convolutional neural network to estimate the phase noise and remove it from the interferogram. This method also demonstrates the improvement given by the denoising on the phase unwrapping procedure. A CNN encoder-decoder approach is used in (Mukherjee et al., 2018) to denoise SAR interferograms, with a two-channel input and output consisting of the real and imaginary part of the interferogram.

Residual learning is used to obtain interferometric phase denoising in (Liu et al., 2021). The CNN architecture is based on the Denoising CNN (DnCNN) framework proposed in (K. Zhang et al., 2017), however uses pre-activation instead, in which batch normalization and the activation function (ReLU) are applied before the weight layers, as opposed to the usual post-activation where the activation function is applied at the end. In terms of evaluation metrics, both PSNR and Number of Phase Unwrapping Errors (NoUE) were used.

The DeepInSAR method (Sun et al., 2020) uses a CNN architecture to extract features from a concatenated input of the real and imaginary components of the noisy phase, and the normalized amplitudes of the two SLC acquisitions to extract features, which are then used to perform phase filtering and coherence estimation simultaneously using two further CNN sub-networks. DeepInSAR outperformed the box car filter and the NL-SAR and NL-InSAR methods both in terms of RMSE and SSIM.

A scale recurrent neural network (RNN) is used in (Pu et al., 2020) to achieve interferometric phase filtering, in which RNN units are used to connect three different-scaled subnetworks based on an encoder-decoder architecture. In this way, global structural phase information contained in the different-scaled feature maps can be used. On the same simulated dataset, the overall performance of this method is better than of DeepInSAR (Sun et al., 2020).

A different approach was taken by (Mukherjee et al., 2020), which used an unsupervised generative model to perform joint phase filtering and coherence estimation, which directly learns the InSAR data distribution, i.e. the bivariate (real and imaginary) Gaussian parameters μ and σ for a centre pixel in a given neighbourhood. The method outperforms the NL-SAR, NL-InSAR, as well as the Goldstein and box car filters in terms of RMSE and computational time.

2.2 Metrics

The majority of the methods reviewed focused on RMSE as a performance metric, followed by PSNR and SSIM, which are standard image processing metrics. However, two papers also presented the Number Of Residues (NOR) (Bamler et al., 1998). Residues are points of two-dimensional phase inconsistency determined by integration of the phase differences around closed paths, and therefore it is desirable to minimize them. Another metric occasionally presented is the phase cosine error.

2.3 Comparison of methods

A comparison of some state-of-the-art phase denoising methods is shown in table 1. As each method evaluated the performance on a different dataset, except in one case, and due to the variety of metrics used, the metrics reported in each of the papers when comparing the method to previous techniques is also reported.

3 Phase Unwrapping

3.1 Methods

Phase unwrapping is a crucial signal processing problem in several applications, such as digital holographic interferometry, SAR and Magnetic Resonance Imaging, in which the aim is to restore the original phase from the wrapped phase. As a result, there are several works both in remote sensing journals as well as in signal and image processing journals. In SAR interferometry, almost all single-baseline phase unwrapping methods exploit the phase continuity assumption (also known as the Itoh condition, which requires that the absolute phase difference between any two neighbouring pixels be less than π Yu et al., 2019. However, system noise and abrupt topographic changes or deformation frequently result in the failure of the Itoh condition in practice. The state-of-the-art currently lies in the use of deep learning techniques with convolutional neural networks (Spoorthi et al., 2019; Wang et al., 2019; Zhou et al., 2020).

As a result, most modern techniques focus on multi-baseline phase unwrapping (MB PU), which is a well-posed problem as it can take advantage of baseline diversity to significantly increase the ambiguity intervals of interferometric phases, and completely overcomes the limitation of the Itoh condition. MB PU methods can be divided into two major groups: parametric and nonparametric methods. The former make use of the InSAR pdf to formulate a maximum likelihood (Fornaro et al., 2006;

Method	Year	Dataset	RMSE (radians)	SSIM	NOR	PSNR (dB)
InSAR-BM3D (Sica et al., 2018)	**2018**	**Simulated data[1]**	**0.2858**	-	**282.18**	-
NL-SAR (Deledalle et al., 2015)	-	Simulated data[1]	0.5045	-	996.95	-
NL-InSAR (Deledalle et al., 2011)	-	Simulated data[1]	0.5358	-	523.30	-
Goldstein (Goldstein et al., 1998)	-	Simulated data[1]	0.7233	-	2662.13	-
Lee (Jong-Sen Lee et al., 1998)	-	Simulated data[1]	0.4973	-	377.03	-
BoxCar (Jong-Sen Lee et al., 1994b)	-	Simulated data[1]	0.5113	-	354.45	-
DeepInSAR (Sun et al., 2020)	**2020**	**Simulated data[2]**	**0.9593**	**0.7976**	-	-
BoxCar (Jong-Sen Lee et al., 1994b)	-	Simulated data[2]	1.2096	0.5150	-	-
NL-SAR (Deledalle et al., 2015)	-	Simulated data[2]	1.2801	. 0.4684	-	-
NL-InSAR (Deledalle et al., 2011)	-	Simulated data[2]	1.1890	0.5202	-	-
GenInSAR (Mukherjee et al., 2020)	**2020**	**Simulated data[3]**	**0.687**	-	-	-
CNN-InSAR (Mukherjee et al., 2018)	-	Simulated data[3]	1.270	-	-	-
NL-SAR (Deledalle et al., 2015)	-	Simulated data[3]	1.537	-	-	-
NL-InSAR (Deledalle et al., 2011)	-	Simulated data[3]	0.850	-	-	-
Goldstein (Goldstein et al., 1998)	-	Simulated data[3]	1.260	-	-	-
BoxCar (Jong-Sen Lee et al., 1994b)	-	Simulated data[3]	1.025	-	-	-
SRN (Pu et al., 2020)	**2020**	**Simulated data[4]**	**0.6340**	**0.8811**	**0.004**	-
Lee (Jong-Sen Lee et al., 1998)	-	Simulated data[4]	1.5372	0.2008	369	-
Goldstein (Goldstein et al., 1998)	-	Simulated data[4]	1.2182	0.4617	16	-
InSAR-BM3D (Sica et al., 2018)	-	Simulated data[4]	0.9070	0.7366	0.012	-
SRN (Pu et al., 2020)	-	**same as DeepInSAR**	**0.6703**	**0.8606**	-	-
DeepInSAR (Sun et al., 2020)	-	same as DeepInSAR	0.8536	0.8666	-	-
In-CNN (Liu et al., 2021)	**2021**	**Simulated data[5]**	-	-	-	**39.183**
WFT (Kemao, 2007)	-	Simulated data[5]	-	-	-	36.352
In-BM3D (W. Zhang et al., 2014)	-	Simulated data[5]	-	-	-	34.957
SP (Hongxing et al., 2015)	-	Simulated data[5]	-	-	-	37.019
GS	-	Simulated data[5]	-	-	-	37.082
DnCNN (K. Zhang et al., 2017)	-	Simulated data[5]	-	-	-	35.633
ComCSC-GR (Kang et al., 2021)	**2021**	**Simulated data[6]**	-	-	-	**31.140**
InSAR-BM3D (Sica et al., 2018)	-	Simulated data[6]	-	-	-	30.575
ComCSC (Kang et al., 2021)	-	Simulated data[6]	-	-	-	26.975
NL-SAR (Deledalle et al., 2015)	-	Simulated data[6]	-	-	-	27.830
NL-InSAR (Deledalle et al., 2011)	-	Simulated data[6]	-	-	-	28.658
Goldstein (Goldstein et al., 1998)	-	Simulated data[6]	-	-	-	19.203
BoxCar (Jong-Sen Lee et al., 1994b)	-	Simulated data[6]	-	-	-	24.685

[1] Average performance on cones, peaks, ramps and squares
[2] High AWGN, with low amplitude strips and high fringe frequency level (S2-S-F3)
[3] Gaussian bubbles, roads and buildings
[4] Generated using Gaussian distributed random matrix
[5] Mountains (Gaussian $\sigma = 0.5$)
[6] Average performance on mountains, peaks, shear plane, squares

Table 1: Summary of the performance of recent interferometric phase denoising methods.

Pascazio et al., 2002) or maximum a posteriori framework (Ferraiuolo et al., 2004; Fornaro et al., 2002; Poggi et al., 2000), while the latter make use of unsupervised learning techniques to estimate absolution phase. Typically, clustering algorithms are used to group pixels with the same 2π-ambiguity, such that the cluster centroid can then be used to estimate the terrain heights of all pixels in the same cluster (Yu et al., 2011).

A new processing flow is proposed in (Wu et al., 2020), in which the authors develop two CNNs for fast detection of deformation caused by mining (DDNet) followed by phase unwrapping (PUNet). The training dataset of phase interferograms was developed by simulating the three components (deformation phase, turbulent atmospheric phase and decorrelation noise) independently and then superimposing them together to get the final simulated phase. A distorted 2D Guassian surface was used to simulate the deformation phase, which results in a typical bell shape representing the ground subsidence caused by mining. They compared the performance of the StaMPS (Hooper et al., 2004) method to the PUNet in extracting Persistent Scatterer (PS) points, and found that the PUNet method was able to estimate the maximum subsidence rate much better than the StaMPS method.

The problem of phase unwrapping is tackled from a semantic segmentation point of view in (Sica et al., 2020). A U-Net architecture is used to map the phase interferogram and coherence to the range/azimuth wrap count gradient, which can then be used to derive the unwrapped phase field. The coherence is useful as an additional input feature as it helps the network to identify and manage critical noisy regions. When compared to other methods, such as Statistical-Cost, Network-Flow Algorithm for Phase Unwrapping (SNAPHU) (C. W. Chen et al., 2002) and PU via MAx flows (PUMA) (Bioucas-Dias et al., 2007), it performs better in terms of RMSE. A U-Net architecture is also used in (Z. Zhang et al., 2020) to estimate the number of integer multiples of 2π (ambiguity number) to add to the wrapped phase.

3.2 Metrics

The vast majority of papers make use of the RMSE in order to quantify performance.

3.3 Comparison of methods

A comparison of some state-of-the-art phase unwrapping methods is shown in table 2. As each method evaluated the performance on a different dataset, the metrics reported in each of the papers when comparing the method to previous techniques is also reported.

4 Application of InSAR phase denoising and unwrapping techniques

On 24-27 December 2018, an eruption of Mount Etna took place, resulting from a complex interaction between tectonic and volcanic processes on the volcano's flanks. We have repeated the DInSAR analysis presented in (De Novellis et al., 2019) to show the intermediate stages of the procedure, from the generation of the interferogram to the subsequent filtering, phase unwrapping and finally estimation of displacement.

Two Sentinel-1 SLC acquisitions in descending orbit from the 22nd and the 28th December 2018 respectively were downloaded from the Copernicus hub[1]. Each Sentinel-1 SLC acquisition is divided into three subswaths, and each subswath is made up of 9 bursts. As Mount Etna straddles two subswaths (IW1 and IW2), the SNAP application was used to extract the appropriate bursts, co-register the two acquisitions and generate the interferogram from the phase difference of the two merged subswaths (see figure 1(a)). The flat-earth phase due to the Earth's curvature and the topographic phase contribution are subtracted to produce the final interferogram. Following this, the Goldstein filter was used to denoise the interferogram (see figure 2).

In the interferogram, the phase is wrapped in the range $(-\pi, \pi]$. Therefore, the SNAP application is used to unwrap the phase using the Minimum Cost Flow algorithm (see figure 2(a)). The relation between unwrapped phase (in radians) and displacement (in metres) is given by:

$$d = -\frac{\lambda}{4\pi}\Delta\phi_d \qquad (1)$$

where λ is the wavelength of Sentinel-1's C-band SAR, and $\Delta\phi_d$ is the unwrapped phase, is then used to obtain the deformation map shown in figure 2(b). This map shows evidence of up to 25 cm of subsidence on the eastern side, and up to 20 cm of uplifting on the western side.

5 Summary

This paper has reviewed the state-of-the-art in SAR interferometric phase denoising and unwrapping. In the Coastal SAGE project, we aim to go beyond the state-of-the-art in interferometric SAR denoising by considering deep learning specifically for the problem of generating noise-reduced interferometric phase. The enhanced quality interferograms will preserve spatial resolution, allowing for more detailed displacement and deformation monitoring using standard PSI techniques. Deep learning architectures will also be used to tackle single-baseline

[1]https://scihub.copernicus.eu

Method	Year	Dataset	RMSE (radians)	Phase Error (radians)
PhaseNet (Spoorthi et al., 2019)	**2019**	**Simulated data[1]**	**1.414**	-
QGPU (Ghiglia et al., 1998)	-	Simulated data[1]	3.317	-
MATLAB's Unwrap (MATLAB, 2022)	-	Simulated data[1]	4.123	-
LPM-TSPA (Lan et al., 2019)	**2019**	**Simulated data[2]**	**1.030**	-
L1-Norm (Costantini, 1998)	-	Simulated data[2]	1.122	-
TSPA (Yu et al., 2016)	-	Simulated data[2]	1.319	-
CNN+ (Sica et al., 2020)	**2020**	**Real data[3]**	**3.90**	-
CNN (Sica et al., 2020)	-	Real data[3]	4.52	-
Branch Cut (Goldstein et al., 1988)	-	Real data[3]	10.05	-
LS (Ghiglia et al., 1994)	-	Real data[3]	8.77	-
PUMA (Bioucas-Dias et al., 2007)	-	Real data[3]	4.62	-
SNAPHU (C. W. Chen et al., 2002)	-	Real data[3]	4.08	-
Region Segmentation (Z. Zhang et al., 2020)	**2020**	**Simulated data[4]**	-	**-0.0113**
Least Squares (Ghiglia et al., 1994)	-	Simulated data[4]	-	0.9035
Network Flow (Costantini, 1998)	-	Simulated data[4]	-	0.3448
Branch Cut (Goldstein et al., 1988)	-	Simulated data[4]	-	0.0524
PGNet-PU (Zhou et al., 2020)	**2020**	**Simulated data[5]**	**0.0181[6]**	-
Branch Cut (Goldstein et al., 1988)	-	Simulated data[5]	0.1981[6]	-
MCF (Costantini, 1998)	-	Simulated data[5]	0.0430[6]	-
SNAPHU (C. W. Chen et al., 2002)	-	Simulated data[5]	0.0400[6]	-
PUMA (Bioucas-Dias et al., 2007)	-	Simulated data[5]	0.0408[6]	-
PGNet-PU (Zhou et al., 2020)	**2020**	**Real data[7]**	**0.0088[6]**	-
Branch Cut (Goldstein et al., 1988)	-	Real data[7]	0.1054[6]	-
MCF (Costantini, 1998)	-	Real data[7]	0.0423[6]	-
SNAPHU (C. W. Chen et al., 2002)	-	Real data[7]	0.0283[6]	-
PUMA (Bioucas-Dias et al., 2007)	-	Real data[7]	0.0107[6]	-

[1] Repeated arithmetic operations (additions and subtractions) on Gaussian functions with randomly varying means and variances; SNR = 0 dB.
[2] Simulated DBInSAR dataset for Isolation Peak region of Colorado; short baseline.
[3] Dataset consists of 10 different patches of 512x512 pixels from a real TanDEM-X single-pass interferogram. For each patch the error is computed between the estimated unwrapped phase field and the reference absolute phase, obtained by back-geocoding the SRTM DEM.
[4] 2D Gaussian distribution with multiple peaks and varying means and variances.
[5] Simulated reference terrain height from the SRTM DEM at Lhasa, Tibet
[6] Normalized RMSE
[7] TerraSAR-X-TanDEM-X interferometry image covering Lhasa, Tibet

Table 2: Summary of the performance of recent phase unwrapping methods.

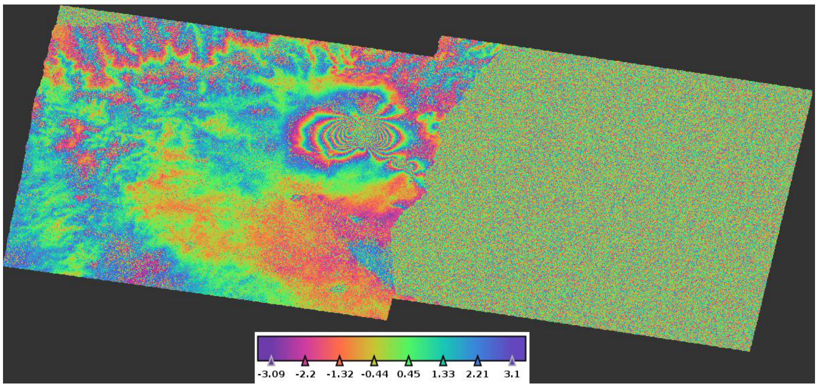

(a) Unfiltered interferogram (radians)

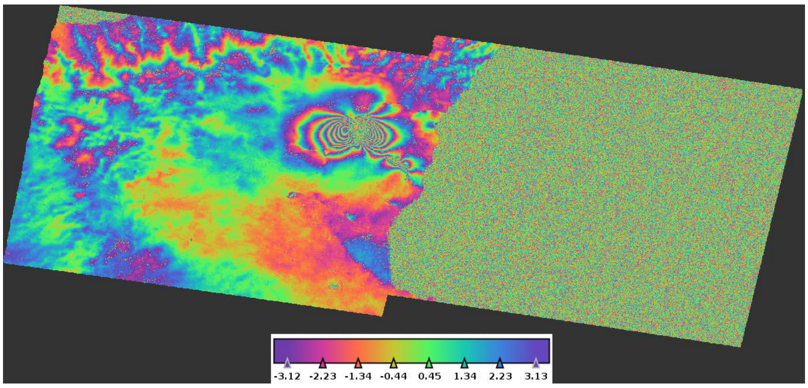

(b) Filtered interferogram (radians)

Figure 1: The original interferogram (a) and filtered interferogram (b) for the case study of the December 2018 Mount Etna eruption.

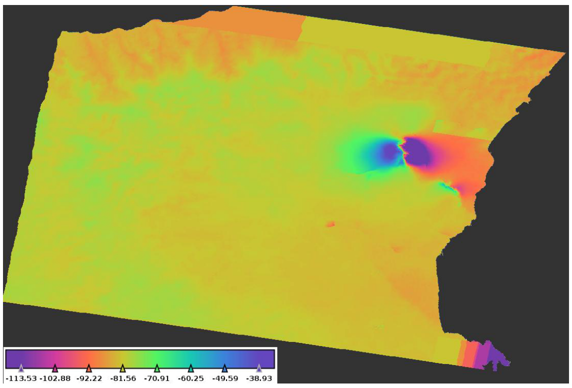

(a) Unwrapped phase (radians)

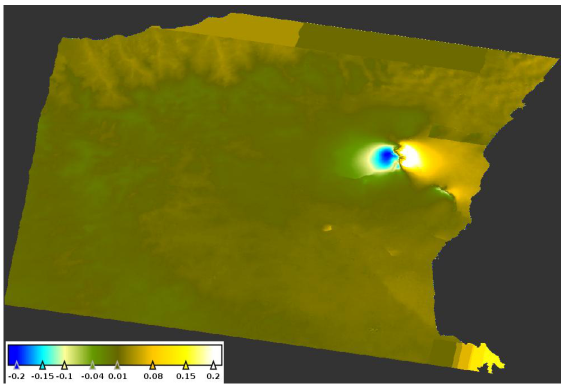

(b) Displacement estimate (metres)

Figure 2: The unwrapped phase (a) and the resulting displacement estimation (b) for the case study of the December 2018 Mount Etna eruption.

and multi-baseline phase unwrapping. The project will integrate the better performing phase denoising and unwrapping methods in the PSI pipeline, and evaluate the quality of the resulting deformation maps with respect to the standard pipeline.

6 Acknowledgements

Project Coastal SAGE financed by the Malta Council for Science & Technology, for and on behalf of the Foundation for Science and Technology, through the Space Research Fund.

References

Bamler, R. & Hartl, P. (1998). Synthetic aperture radar interferometry. *Inverse Problems*, *14*(4), R1–R54.

Bioucas-Dias, J. M. & Valadao, G. (2007). Phase unwrapping via graph cuts. *IEEE Transactions on Image Processing*, *16*(3), 698–709.

Chen, C. W. & Zebker, H. A. (2002). Phase unwrapping for large SAR interferograms: statistical segmentation and generalized network models. *IEEE Transactions on Geoscience and Remote Sensing*, *40*(8), 1709–1719.

Chen, R., Yu, W., Wang, R., Liu, G. & Shao, Y. (2013). Interferometric phase denoising by pyramid nonlocal means filter. *IEEE Geoscience and Remote Sensing Letters*, *10*(4), 826–830.

Costantini, M. (1998). A novel phase unwrapping method based on network programming. *IEEE Transactions on Geoscience and Remote Sensing*, *36*(3), 813–821.

De Novellis, V., Atzori, S., De Luca, C., Manzo, M., Valerio, E., Bonano, M., Cardaci, C., Castaldo, R., Di Bucci, D., Manunta, M., Onorato, G., Pepe, S., Solaro, G., Tizzani, P., Zinno, I., Neri, M., Lanari, R. & Casu, F. (2019). Dinsar analysis and analytical modeling of mount etna displacements: The december 2018 volcano-tectonic crisis. *Geophysical Research Letters*, *46*(11), 5817–5827.

Deledalle, C., Denis, L. & Tupin, F. (2009). Iterative weighted maximum likelihood denoising with probabilistic patch-based weights. *IEEE Transactions on Image Processing*, *18*(12), 2661–2672.

Deledalle, C., Denis, L. & Tupin, F. (2011). NL-InSAR: Nonlocal Interferogram Estimation. *IEEE Transactions on Geoscience and Remote Sensing*, *49*(4), 1441–1452.

Deledalle, C., Denis, L., Tupin, F., Reigber, A. & Jäger, M. (2015). NL-SAR: A Unified Nonlocal Framework for Resolution-Preserving (Pol)(In)SAR Denoising. *IEEE Transactions on Geoscience and Remote Sensing*, *53*(4), 2021–2038.

European Space Agency. (2012). Sentinel-1: ESA's Radar Observatory Mission for GMES Operational Services.

European Space Agency. (2022). Copernicus Open Access Hub, available online at: https://scihub.copernicus.eu.

Ferraiuolo, G., Pascazio, V. & Schirinzi, G. (2004). Maximum a posteriori estimation of height profiles in InSAR imaging. *IEEE Geoscience and Remote Sensing Letters*, *1*(2), 66–70.

Ferretti, A., Fumagalli, A., Novali, F., Prati, C., Rocca, F. & Rucci, A. (2011). A New Algorithm for Processing Interferometric Data-Stacks: SqueeSAR. *IEEE Transactions on Geoscience and Remote Sensing*, *49*(9), 3460–3470.

Fornaro, G., Guarnieri, A., Pauciullo, A. & Dezan, F. (2006). Maximum likelihood multi-baseline SAR interferometry. *Proc. Inst. Electr. Eng., vol. 153, no. 3, pp. 279–288*.

Fornaro, G., Pauciullo, A. & Sansosti, E. (2002). Bayesian approach to phase-difference-based phase unwrapping. *Conference Record of the Thirty-Sixth Asilomar Conference on Signals, Systems and Computers, 2002.*, *2*, 1391–1396 vol.2.

Ghiglia, D. C. & Pritt, M. D. (1998). *Two-Dimensional phase unwrapping: Theory, algorithms and software*. WileyBlackwell.

Ghiglia, D. C. & Romero, L. A. (1994). Robust two-dimensional weighted and unweighted phase unwrapping that uses fast transforms and iterative methods. *J. Opt. Soc. Am. A*, *11*(1), 107–117.

Goldstein, R. M., Zebker, H. A. & Werner, C. L. (1988). Satellite radar interferometry: Two-dimensional phase unwrapping. *Radio Science*, *23*(4), 713–720.

Goldstein, R. M. & Werner, C. L. (1998). Radar interferogram filtering for geophysical applications. *Geophysical Research Letters*, *25*(21), 4035–4038.

Hongxing, H., Bioucas-Dias, J. M. & Katkovnik, V. (2015). Interferometric phase image estimation via sparse coding in the complex domain. *IEEE Transactions on Geoscience and Remote Sensing*, *53*(5), 2587–2602.

Hooper, A., Zebker, H., Segall, P. & Kampes, B. (2004). A new method for measuring deformation on volcanoes and other natural terrains using InSAR persistent scatterers. *Geophysical Research Letters*, *31*(23).

Jong-Sen Lee, Hoppel, K. W., Mango, S. A. & Miller, A. R. (1994a). Intensity and phase statistics of multilook polarimetric and interferometric SAR imagery. *IEEE Transactions on Geoscience and Remote Sensing*, *32*(5), 1017–1028.

Jong-Sen Lee, Hoppel, K. W., Mango, S. A. & Miller, A. R. (1994b). Intensity and phase statistics of multilook polarimetric and interferometric SAR imagery. *IEEE Transactions on Geoscience and Remote Sensing*, *32*(5), 1017–1028.

Jong-Sen Lee, Papathanassiou, K. P., Ainsworth, T. L., Grunes, M. R. & Reigber, A. (1998). A new technique for noise filtering of SAR interferometric phase images. *IEEE Transactions on Geoscience and Remote Sensing*, *36*(5), 1456–1465.

Kang, J., Hong, D., Liu, J., Baier, G., Yokoya, N. & Demir, B. (2021). Learning convolutional sparse coding on complex domain for interferometric phase restoration. *IEEE Transactions on Neural Networks and Learning Systems*, *32*(2), 826–840.

Kemao, Q. (2007). Two-dimensional windowed Fourier transform for fringe pattern analysis: Principles, applications and implementations [Phase Measurement Techniques and their applications]. *Optics and Lasers in Engineering*, *45*(2), 304–317.

Lan, Y., Yu, H. & Xing, M. (2019). Refined two-stage programming-based multi-baseline phase unwrapping approach using local plane model. *Remote Sensing*, *11*(5).

Li, S., Xu, H., Gao, S. & Li, C. (2019). Non-fuzzy interferometric phase estimation method based on deep learning. *IGARSS 2019 - 2019 IEEE International Geoscience and Remote Sensing Symposium*, 194–197.

Lin, X., Li, F., Meng, D., Hu, D. & Ding, C. (2015). Nonlocal SAR Interferometric Phase Filtering Through Higher Order Singular Value Decomposition. *IEEE Geoscience and Remote Sensing Letters*, *12*(4), 806–810.

Liu, B., Wu, L., Hao, H. & Dong, J. (2021). Interferometric phase image denoising method via residual learning. *Journal of Electronic Imaging*, *30*(2), 1–18.

MATLAB. (2022).

Mukherjee, S., Zimmer, A., Kottayil, N. K., Sun, X., Ghuman, P. & Cheng, I. (2018). CNN-Based InSAR Denoising and Coherence Metric. *2018 IEEE SENSORS*, 1–4.

Mukherjee, S., Zimmer, A., Sun, X., Ghuman, P. & Cheng, I. (2020). An Unsupervised Generative Neural Approach for InSAR Phase Filtering and Coherence Estimation. *IEEE Geoscience and Remote Sensing Letters*, 1–5.

Pascazio, V. & Schirinzi, G. (2002). Multifrequency InSAR height reconstruction through maximum likelihood estimation of local planes parameters. *IEEE Transactions on Image Processing*, *11*(12), 1478–1489.

Poggi, G., Ragozini, A. R. P. & Servadei, D. (2000). A Bayesian approach for SAR interferometric phase restoration. *IGARSS 2000. IEEE 2000 International Geoscience and Remote Sensing Symposium. Taking the Pulse of the Planet: The Role of Remote Sensing in Managing the Environment. Proceedings (Cat. No.00CH37120)*, *7*, 3202–3205 vol.7.

Pu, L., Zhang, X., Zhou, Z., Shi, J., Wei, S. & Zhou, Y. (2020). A Phase Filtering Method with Scale Recurrent Networks for InSAR. *Remote Sensing*, *12*(20).

Seymour, M. S. & Cumming, I. G. (1994). Maximum likelihood estimation for SAR interferometry. *Proceedings of IGARSS '94 - 1994 IEEE International Geoscience and Remote Sensing Symposium*, *4*, 2272–2275 vol.4.

Sica, F., Calvanese, F., Scarpa, G. & Rizzoli, P. (2020). A CNN-Based Coherence-Driven Approach for InSAR Phase Unwrapping. *IEEE Geoscience and Remote Sensing Letters*, 1–5.

Sica, F., Cozzolino, D., Zhu, X. X., Verdoliva, L. & Poggi, G. (2018). InSAR-BM3D: A Nonlocal Filter for SAR Interferometric Phase Restoration. *IEEE Transactions on Geoscience and Remote Sensing*, *56*(6), 3456–3467.

Spoorthi, G. E., Gorthi, S. & Gorthi, R. K. S. S. (2019). PhaseNet: A Deep Convolutional Neural Network for Two-Dimensional Phase Unwrapping. *IEEE Signal Processing Letters*, *26*(1), 54–58.

Sun, X., Zimmer, A., Mukherjee, S., Kottayil, N. K., Ghuman, P. & Cheng, I. (2020). DeepInSAR-A Deep Learning Framework for SAR Interferometric Phase Restoration and Coherence Estimation. *Remote Sensing*, *12*(14).

Wang, K., Li, Y., Kemao, Q., Di, J. & Zhao, J. (2019). One-step robust deep learning phase unwrapping. *Opt. Express*, *27*(10), 15100–15115.

Wu, Z., Zhang, H., Wang, Y., Wang, T. & Wang, R. (2020). A Deep Learning Based Method for Local Subsidence Detection and InSAR Phase Unwrapping: Application to Mining Deformation Monitoring. *IGARSS 2020 - 2020 IEEE International Geoscience and Remote Sensing Symposium*, 20–23.

Yu, H., Lan, Y., Yuan, Z., Xu, J. & Lee, H. (2019). Phase Unwrapping in InSAR : A Review. *IEEE Geoscience and Remote Sensing Magazine*, *7*(1), 40–58.

Yu, H., Li, Z. & Bao, Z. (2011). A cluster-analysis-based efficient multibaseline phase-unwrapping algorithm. *IEEE Transactions on Geoscience and Remote Sensing*, *49*(1), 478–487.

Yu, H. & Lan, Y. (2016). Robust Two-Dimensional Phase Unwrapping for Multibaseline SAR Interferograms: A Two-Stage Programming Approach. *IEEE Transactions on Geoscience and Remote Sensing*, *54*(9), 5217–5225.

Zhang, K., Zuo, W., Chen, Y., Meng, D. & Zhang, L. (2017). Beyond a Gaussian Denoiser: Residual Learning of Deep CNN for Image Denoising. *IEEE Transactions on Image Processing*, *26*(7), 3142–3155.

Zhang, W., Zhang, Q., Zhao, C., YANG, C. & ZOU, W. (2014). Noise reduction for InSAR phase images using BM3D. *Chinese Journal of Electronics*, *23*(2), 329–333.

Zhang, Z., Qian, J., Wang, Y. & Yang, X. (2020). Phase unwrapping via deep learning based region segmentation. *IGARSS 2020 - 2020 IEEE International Geoscience and Remote Sensing Symposium*, 397–400.

Zhou, L., Yu, H. & Lan, Y. (2020). Deep Convolutional Neural Network-Based Robust Phase Gradient Estimation for Two-Dimensional Phase Unwrapping Using SAR Interferograms. *IEEE Transactions on Geoscience and Remote Sensing*, *58*(7), 4653–4665.

Zhu, X. X., Bamler, R., Lachaise, M., Adam, F., Shi, Y. & Eineder, M. (2014). Improving TanDEM-X DEMs by Non-local InSAR Filtering. *EUSAR 2014; 10th European Conference on Synthetic Aperture Radar*, 1–4.